ther studies are necessary to elucidate the observed difference, this analysis demonstrates one of the remarkable feature of FRS that one can measure a *differential* diffusion coefficient provided A_1 and A_2 are known. Indeed, FRS is a very sensitive and versatile technique to measure tracer diffusion coefficient. but it is indispensable for an accurate interpretation of FRS data to know about the optical properties of the probe in the system of interest. It can not be said, however, that appropriate care has been paid so far.

Acknowledgement. This work was financially supported in part by grants from the Ministry of Education and from the Korean Science and Engineering Foundation.

References

1. T. Chang, H. Kim, and H. Yu, *Macromolecules,* **20**, 2629 (1987) and references therein.
2. I. H. Park, C. S. Johnson, Jr., and D. A. Gabriel, *Macromolecules,* **23**, 1548 (1990) and references therein.
3. R. Furukawa, J. L. Arauz-Lara, and B. R. Ware, *Macromolecules,* **24**, 599 (1991) and references therein.
4. P.-G. de Gennes, *Scaling Concepts in Polymer Physics,* Cornell Univ. Press, Ithaca (1979).
5. D. Langevin and F. Rondenlez, *Polymer,* **19**, 875 (1978).
6. R. I. Cukier, *Macromolecules,* **17**, 252 (1984).
7. G. S. Ullman. K. Ullman, R. M. Linder, and G. D. Phillis, *J. Phys. Chem.,* **89**, 652 (1985).
8. J. A. Lee and T. P. Lodge, *J. Phys. Chem.,* **91**, 5546 (1987).
9. H. Hervet, W. Urbach, and F. Rondelez, *J. Chem. Phys.,* **68**, 2725 (1978).
10. J. A. Wesson, H. Takezoe, H. Yu, and S. P. Chen, *J. Appl. Phys.,* **53**, 6513 (1982).
11. H. Sillescu, C. H. Wang, and J. Coutandin, *Macromolecules,* **18**, 587 (1985).
12. D. L. Ross and J. Blanc in *Photochromism*, G. H. Brown ed., Wiley, New York, Chapter 5 (1972).
13. A. V. El'tsov, *Organic photochromes,* Plenum, New York p. 112 (1990)
14. H. Kogelnik, *Bell Syst. Tech. J.,* **48**, 2909 (1969).
15. A. von Jena and H. E. Lessing, *Opt. Quantum Electron.,* **11**, 419 (1979).
16. K. A. Nelson, R. Casalegno, R. J. Dwayne Miller and M. D. Fayer, *J. Chem. Phys.,* **77**, 1144 (1982).
17. H. Kim, T. Chang, J. M. Yohanan, L. Wang, and H. Yu, *Macromolecules,* **19**, 2737 (1986).
18. W. J. Huang, T. S. Frick, M. R. Landry, J. A. Lee, T. P. Lodge, and M. Tirrell, *AICHE J.,* **33**, 573 (1987).
19. L. S. Lever, M. S. Bradley, and C. S. Johnson, Jr., *J. Mag. Res.,* **68**, 335 (1986).
20. W. Urbach, H. Hervet, and F. Rondelez, *J. Chem. Phys.,* **83**, 1877 (1985).
21. M. R. Landry, Q. Gu, and H. Yu, *Macromolecules,* **21**, 1158 (1988).
22. C. S. Johnson, Jr., *J. Opt. Soc. Am. B,* **2**, 317 (1985).
23. H. Kim, Ph. D. Dissertation, University of Wisconsin-Madison (1987).
24. S. Park, J. Sung, H. Kim, and T. Chang. *J. Phys. Chem.,* in press.
25. R. C. Weast ed., *Handbook of Chemistry and Physics, 70th Ed.,* CRC Press (1989).

A Theoretical Study of CO Molecules on Metal Surfaces: Coverage Dependent Properties

Sang -H. Park and Hojing Kim*

Department of Chemistry, Seoul National University, Seoul 151-742. *Received June 26, 1991*

The CO molecules adsorbed on Ni(111) surface is studied in the cluster approximation employing EH method with self-consistent charge iteration. The effect of CO coverage is simulated by allowing the variation of valence state ionization potentials of each Ni atom in model cluster according to the self-consistent charge iteration method. The CO coverage dependent C-O stretching frequency shift, adsorption site conversion, and metal work function change are attributed to the charge transfer between metal surface and adsorbate. For CO/Ni(111) system, net charge transfer from Ni surface to chemisorbed CO molecules makes surface Ni atoms be more positive with increasing coverage, and lowers Ni surface valence band. This leads to a weaker interaction between metal surface valence band and Co $2\pi^*$ MO, less charge transfer to a single CO molecule, and the bule shift of C-O stretching frequency. Further increase of coverage induces the conversion of 3-fold site CO to lower coordination site CO as well as the blue shift of C-O stretching frequency. This whole process is accompanied by the continuous increase of metal work function.

Introduction

One of the most extensively studied adsorbates is carbon monoxide. Its interaction with metal surfaces has constituted the model systems for molecular chemisorption for many years. When a CO molecule is adsorbed on a metal surface, the vibrational frequency ω_{CO} of the intramolecular stretching mode exhibits substantial downward shift from its gas phase value at 2143 cm^{-1}. It has been widely accepted that the 5σ orbital of the CO molecule is primarily responsible for

the chemical bond formation to the substrate.[1,2] Since the 5σ orbital is essentially a lone-pair orbital on the carbon atom, it has been suggested that the donation of the 5σ electrons to the metal is simultaneously accompanied by back-donation in the $2\pi^*$ orbitals of the chemisorbed CO, which is the lowest unoccupied level in the gas phase. The degree of each charge transfer depends on the electronic properties of the adsorbate, and also play a significant role in the change of the vibrational properties upon chemisorption. Since the $2\pi^*$ orbitals have an anti-bonding character with respect to the molecular interatomic bond, the partial occupancy weakens the C-O bond strength. This leads to the elongation of the C-O bond distance, and to the decrease in ω_{CO} compared to the neutral CO molecule in the gas phase.[3]

There is, in general, an additional coverage dependent shift of the vibrational frequency. It has been reported that the vibrational frequency of CO adsorbed on Ru, Pd, Ni surfaces increase with increasing CO coverage.[4-9] These upward frequency shifts have been explained in terms of the dipole-dipole coupling theory,[10-12] in which each molecule experiences the electric field not only of the incident photons, but also of the surrounding vibrating dipoles of the adsorbed molecules.

It has been proposed that there is another component to this coverage dependent frequency shift. This is known as the chemical shift.

The dipole coupling shift and the chemical shift contribution can be seperated experimentally in IRAS (Infrared Absorption Spectroscopy) by the use of isotopic mixtures. While neighboring molecules with identical frequencies experience dipole coupling, molecules with sufficiently different frequencies can be considered vibrationally decoupled.[13]

The chemisorption of CO by the Ni(111) surface provides a classical example of multiple CO coordination possibilities to surface Ni atoms. Early studies suggested that up to a coverage of one-half only the 2-fold sites are occupied.[14,15] This simple picture of chemisorption has been challenged by IRAS and HREELS (High Resoltion Electron Energy Loss Spectroscopy). The C-O stretching frequencies obtained by these techniques revealed a much more complicated situation.[16,17] At low coverage, only the 3-fold sites are populated. With increase in coverage, a continuous conversion from the 3-fold to 2-fold site occurs. This transformation is completed when coverage is about 0.16. Terminally bonded CO can be observed whenever coverage is greater than 0.3.[18,19] It has been also reported that CO adsorbed on 3-fold site shows slight upward frequency shift, and that CO on 2-fold site shows strong upward frequency shift.[19]

In this work, coverage dependent frequency shift of CO adsorbed on Ni(111) surface is studied employing Extended Hückel (EH) method with self-consistent charge iteration.[20,21] The effect of different CO coverage is simulated by allowing the variation of the energy parameters (H_{ii}) of each Ni atom. These variation of the energy parameters of Ni were performed for each model cluster by using self-consistent charge iteration method on each Ni atoms. Anderson have proposed valence state ionization potential shift approach to explain various surface phenomena.[22-26] He has simulated the effects of adsorbate or applied potential on surface by the variation of metal energy parameters. He has varied arbitrarily the valence state ionization potential (VSIP) of all metal atoms

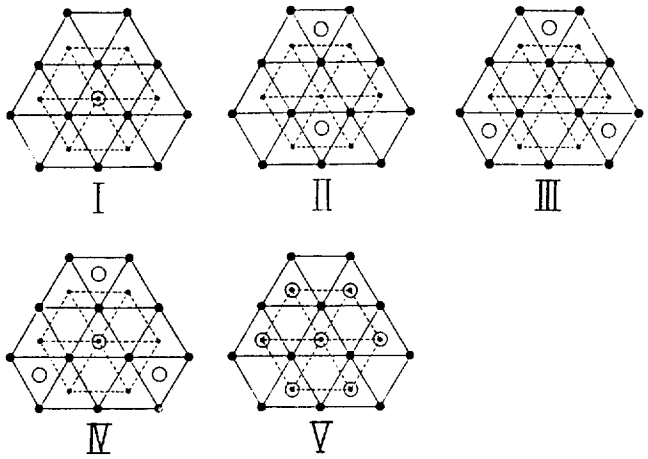

Figure 1. Model clusters for CO/Ni(111) system. The large white circles are CO molecules, the large black circles surface Ni atoms, and the small black circles second layer Ni atoms.

in same quantity within the framework of molecular orbital theory. In contrast to the Anderson's approach, self-consistent charge iteration method is employed in determining the energy parameters of each metal atom for each system.

Due to the net charge transfer between adsorbed CO and Ni substrate, increase of CO coverage moves the energy parameters of surface Ni atoms to lower energy. This change of metal atom energy parameters is used to explain the coverage dependent metal work funtion changes, coverage dependent frequency shifts, adsorption site preferences and the interrelations among these.

In addition to the CO chemisorption on Ni(111) surface, CO adsorbed on Pt(111) surface was also considered for the comparison purpose. For the CO/Pt(111) system, the observed C-O stretching frequency suggested that up to CO coverage 0.3, only the on-top site was occupied.[27] As coverage increase to 0.5, one-half of the CO molecules are located at the on-top site while the other half adsorb on the 2-fold site.[28] More recent study by IRAS, however, has indicated that the 2-fold site of Pt(111) surface begins to be populated when the CO coverage is around 0.2-0.3.[29] These experimental results have been also supported by Monte Carlo simulation.[30,31]

Although the limitation of EH method confines this study to only a qualitative investigation, it reveals some trends of above mentioned phenomena.

Computation

Model Clusters and its Geometries. Model clusters used in present work for the CO/Ni(111) system are given in Figure 1. Ni-Ni distances were fixed at bulk value of 2.49 Å for each model cluster. The Ni-C and C-O bond lenghs in the Ni(111)-($\sqrt{3}\times\sqrt{3}$)R30°-CO system have been determined by normal photoelectron diffraction (NPD) to be 1.78 ± 0.03 and 1.13 Å, respectively.[32] For the surface structure Ni(100)-c(2×2)-CO, in which only the on-top site have been populated, the Ni-C distance is about 1.71 Å.[33-35] In organonickel carbonyls, the Ni-C bonds are usually bracketed in the range of 1.69-1.86 Å for terminal CO, 1.83-1.98 Å for μ_2-CO, and 1.89-2.03 Å for μ_3-CO.[36-38] Considering these experi-

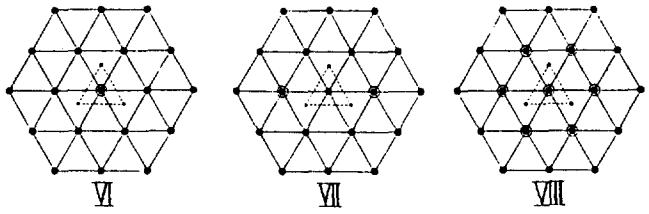

Figure 2. Model clusters for CO/Pt(111) system. The large white circles are CO molecules, the large black circles surface Pt atoms, and the small black circles second layer Pt atoms.

mental data, the Ni-C bond lengths are taken to be 1.71, 1.87, 1.96 Å for on-top, 2-fold, and 3-fold adsorption sites. The C-O bond length is kept fixed at 1.13 Å for all adsorption sites. These geometries are the same as that of Wong and Hoffmann[39] except Ni-C bond length for 2-fold adsorption site. In their paper, the 2-fold site has been calculated to be the most stable one because they has simulated the Ni(111)-($\sqrt{3}\times\sqrt{3}$)R30°-CO system. CO adsorbed on 2-fold site has been found experimentally to be the most strongly adsorbed one at this CO coverage. It has been reported, however, that the 3-fold site was the most stable one with the calculated site preference order 3-fold>2-fold>1-fold at a very low CO coverage.[40] This is consistent with vibrational analysis of Campuzano and Greenler,[41] and with that of Surnev and Xu.[42] Since the binding energy calculated by EH method depends strongly on Ni-C bond length, without any significant change of interaction scheme, slight change 0.06 Å of Ni-C length for 2-fold adsorption site from the Wong and Hoffmann's value is made to have the site preference 3-fold>2-fold>1-fold at a very low CO coverage.

Model clusters given in Figure 2 are used in this paper for the CO/Pt(111) system. Pt-Pt distances are kept fixed at bulk value of 2.77 Å for each model cluster. The Pt(111)-c(4×2)-2CO surface structure has been investigated in detail by dynamical LEED, in which one-half of the CO molecules are located at the on-top site while the other half are adsorbed on the 2-fold site. The Pt-C bond lengths have been reported to 1.85 and 2.08 Å respectively for the on-top and 2-fold bridge site.[43] The C-O bond length is kept fixed at 1.15 Å for all adsorption site.

Methodology. Extended Hückel calculation with charge iteration on metal atoms is performed to calculate molecular orbitals of the model clusters given in Figure 1 and 2, assuming a quadratic dependence of metal H_{ii}'s on its charge. It has been known that the results of self-consistent charge iteration usually show a marked improvement over the results obtained without iteration.[20,21,44]

Diagonal Hamiltonian matrix elements of metal atoms are set up as follows. The term valence state ionization potentials (VSIP) denotes the energy necessary to remove an electron from a given orbital of either a specific configuration or valence configuration.

$$H_{ii} = -\mathrm{VSIP}_i(Q) = -A_iQ^2 - B_iQ - C_i \qquad (1)$$

The parameter set A_i, B_i, and C_i is usually determined through the atomic spectra data. Net charge Q of an atom α in a molecule is defined as follows.

$$Q = (\text{Number of valence electron of atom } \alpha)$$

Table 1. C and O Atomic Orbital Exponents and H_{ii}

Atom	Orbital	H_{ii} (eV)	ζ
C[a]	2*s*	−21.40	1.6250
	2*p*	−11.40	1.6250
O[a]	2*s*	−32.30	2.2750
	2*p*	−14.80	2.2750

[a] Orbital exponents ζ, and energy parameters (H_{ii}) for C and O atoms are taken from reference 45.

Table 2. Ni and Pt Atomic Orbital Exponents

Atom	Orbital	ζ_1	ζ_2	c_1	c_2
Ni	4*s*[a]	1.8250			
	4*p*[a]	1.1250			
	3*d*[b]	5.7500	2.0000	0.56830	0.62920
Pt[c]	6*s*	2.5500			
	6*p*	2.5500			
	5*d*	6.0100	2.7000	0.63213	0.55186

[a] From reference 46. [b] From reference 47. [c] From reference 48.

Table 3. VSIP Parameters of Ni and Pt Atomic Orbitals (eV)

Atom	Orbital	*A*	*B*	*C*
Ni[a]	4*s*	0.9110	8.5610	7.5400
	4*p*	0.9860	6.5520	3.8900
	3*d*	1.7600	13.5600	10.9000
Pt[b]	6*s*	1.0500	5.1120	8.7280
	6*p*	0.9500	3.8920	5.2090
	5*d*	2.3310	8.5220	12.0020

[a] From reference 49 and 50. [b] From reference 51 and 52.

$$-\left[\sum_{j\in\alpha}\sum_{k}\sum_{i} n_i C^*_{ji} C_{ki} S_{jk}\right] \qquad (2)$$

$$H_{ij} = \frac{k}{2} S_{ij}(H_{ii} + H_{jj}) \qquad (3)$$

k = constant (1.75)

S_{ij} = overlap between i and j atomic orbitals

The parameters used in this work is given in Table 1-3. Energy parameters H_{ii} of metal atoms are not given becouse CO coverage effect is simulated through the variation of H_{ii}'s of each metal atom employing self-consistent charge iteration method. That is, H_{ii}'s of each metal atoms are determined by CO coverage so that H_{ii}'s of each metal atom is different from each model cluster.

The result of calculation for NiCO triatomic molecule employing above parameters are compared with that of *ab initio* effective core potential (ECP) SCF calculation of Rohlfing and Hay[53] to test the reliability of parameters, geometries, and self-consistent charge iteration method itself. Table 4 shows some calculated quantities and their comparison with the ECP SCF results.

Binding energy of Ni-CO is calculated to be 3.82 eV in our calculation compared with 4.05 eV of above mentioned *ab initio* ECP SCF calculation of Rohlfing and Hay. For re-

Table 4. Comparison of the Results of EH Caulation Employing Parameters of This Work and The Result of Effective Core Potential SCF Calculation from Reference 53 for The Ni-C Bond Length of NiCO Molecule and Mulliken Populations

	Ni-C	Ni			C		O	
	Å	*s*	*p*	*d*	*s*	*p*	*s*	*p*
EHT	1.710	0.44	0.10	9.37	3.32	2.07	3.62	5.07
ECP[a]	1.711[b]	0.43	0.09	9.57	3.59	1.95	3.90	4.46

[a] *ab initio* effective core potential SCF calculation of reference 53. [b] Geometry optimized value from reference 53.

ference, experimentally determined Ni-CO binding energy in gas phase has been reported to be 2.32-3.62 eV.[54]

Our concern is mainly on the role of CO 5σ (HOMO) and CO 2π* (LUMO) molecular orbitals when CO molecules interact with metal surface. So, the contribution of each CO molecular orbital must be isolated from the calculated molecular orbitals of total system. Basis transformation from Ni, C, O atomic orbital basis to the CO molecular orbital and Ni cluster molecular orbital basis is performed to meet this needs. In the case of model cluster II Figure 1, for example, CO molecular orbitals and Ni_{19} cluster molecular orbitals are calculated seperately using the same energy parameters (H_{ii}) and geometries. And then, transformation is performed taking above fragment molecular orbitals as basis. The transformation is expressed as follows.

$$\Psi_i=\sum_j C_{ji}\varphi_j=\sum_k C'_{ki}\varphi'_k \tag{4}$$

In Eq. (4), Ψ_i is a molecular orbital of total system, φ_j is a atomic orbital basis, and φ'_k is the fragment molecular orbital basis which are consisted of CO molecular orbitals and Ni_{19} molecular orbitals in the case of model cluster I-V.

The density of states (DOS) curve given in Eq. (5) is a plot of the number of orbitals per unit energy as abscissa, versus energy as ordinate. This DOS curve is resolved into the projected DOS (PDOS). $PDOS_A$, for example, represents the contribution of an atom *A* to the total DOS.

DOS (Density of States)

$$=\sum_i \delta(E-E_i)\langle\Psi_i|\Psi_i\rangle$$

$$=\sum_i \delta(E-E_i)\sum_j\sum_k C_{ji}C_{ki}S_{jk}$$

$$=\sum_j\left(\sum_i \delta(E-E_i)\sum_k C_{ji}C_{ki}S_{jk}\right)$$

$$=\sum_{j\in A}\left(\sum_i \delta(E-E_i)\sum_k C_{ji}C_{ki}S_{jk}\right)+\sum_{j\in B}\left(\sum_i \delta(E-E_i)\sum_k C_{ji}C_{ki}S_{jk}\right)$$

$$+\sum_{j\in C}\left(\sum_i \delta(E-E_i)\sum_k C_{ji}C_{ki}S_{jk}\right)+\cdots\cdots$$

$$=PDOS_A+PDOS_B+PDOS_C+\cdots\cdots \tag{5}$$

As the analogue of overlap population (OP) which indicates bond strength between adjacent atoms in a molecule, fragment overlap population (FOP) is defined as follows utilizing C'_{ki} of Eq. (4)

$$FOP=2\sum_i n_i\sum_{j\in\alpha}\sum_{k\in\beta}C'_{ji}C'_{ki}S'_{jk} \tag{6}$$

In Eq. (6), α is metal substrate fragment and β is CO molecule fragment. FOP defined in Eq. (6) can be interpreted as representing bond strength between a CO molecule and a metal substrate.

FOP is resolved into the contribution of each CO molecular orbitals as in Eq. (7). $FOP_{2\pi(x)}+FOP_{2\pi(y)}$ and $FOP_{5\sigma}$ in Eq. (7) represents the contribution of CO 2π* and CO 5_σ molecular orbital to the CO-metal bond strength respectively.

$$FOP=\sum_{k\in\beta}\left(2\sum_i n_i\sum_{j\in\alpha}C'_{ji}C'_{ki}S'_{jk}\right.$$

$$=FOP_{6\sigma}+FOP_{2\pi(x)}+FOP_{2\pi(y)}+FOP_{5\sigma}+FOP_{1\pi(x)}$$

$$+FOP_{1\pi(y)}+FOP_{4\sigma}+FOP_{3\sigma} \tag{7}$$

The crystal orbital overlap population (COOP) curve is a plot of the overlap-population-weighted density of states versus energy. Integration of the COOP curve up to the Fermi energy gives the total overlap population. The positive regions of the COOP curve represent bonding and the negative regions antibonding. The amplitude of the COOP curve depends on the number of states in an energy interval, the magnitude of the coupling overlap, and the size of the coefficients in the MO's.[55] While the COOP curve is defined between adjacent atoms in a molecule, fragment COOP (FCOOP) which represents the characteristics of bonding between fragment is defined as Eq. (8). The intergration of FCOOP up to the Fermi level gives FOP.

FCOOP (Fragment Crystal Orbital Overlap Population)

$$=\sum_i 2\,\delta(E-E_i)\sum_{j\in\alpha}\sum_{k\in\beta}C'_{ji}C'_{ki}S'_{jk}$$

Table 5. Results of Calculation for The Ni_{19}-$(CO)_n$ System

No.[a]	$H_{ii}(d)$[b]	$FOP^c_{2\pi(x)}$	$FOP^c_{2\pi(y)}$	$FOP^c_{5\sigma}$	$\langle n_{2\pi}\rangle^d$	$OP^e_{C\text{-}O}$
I	−11.95174	0.31370	0.31369	0.36178	1.1288	1.1259
II	−12.11655	0.28274	0.26764	0.36482	0.9302	1.1479
III	−12.16872	0.27747	0.26336	0.36635	0.9074	1.1793
IV	−12.85806	0.26816	0.26170	0.36706	0.8784	1.1842
V	−13.59301	0.20109	0.20109	0.31449	0.7445	1.2228

[a] CO coverage increases as one goes down the column. see Figure 1. [b] Converged H_{ii} value of the *d*-orbital of Ni atom at surface center. [c] FOP is defined in Eq. (6) and (7); see text. [d] Partial electron occupation numbers of CO 2π* level. [e] Overlap population between C and O atom. $OP_{C\text{-}O}$ of free CO molecule is 1.3641. Increase of $OP_{C\text{-}O}$ means the blue shift of C-O stretching frequency with increasing coverage.

Table 6. Net Charge[a] of Ni_{19} and CO Fragment of the Ni_{19}-$(CO)_n$ System

No.	Ni_{19}	Center CO	Boundary CO
I	+0.5982	−0.5982	−
II	+0.9116	−	−0.4558
III	+1.1147	−	−0.3716
IV	+1.3545	−0.3360	−0.3395
V	+1.7348	−0.1388	−0.2660

[a]The definition of net charge is given in Eq. (2). Sum of net charges of Ni_{19}, center CO, and boundary CO multiplied by its number becomes zero because the total systems are neutral model clusters.

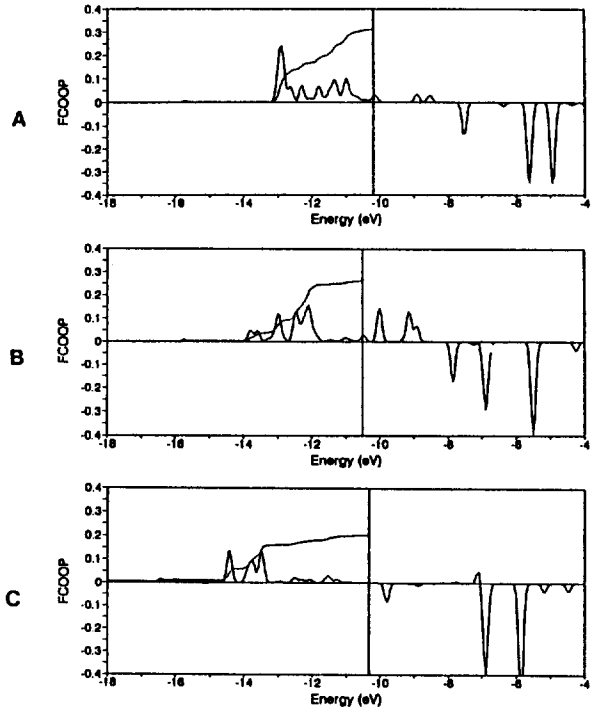

Figure 3. $FCOOP_{2\pi(x)}$ curve defined in Eq. (8) for Ni_{19}-$(CO)_n$ systems. A. model cluster I, B. model cluster IV, C. model cluster V. The vertical lines around 10 eV denote the HOMO energies. The dotted curves are intergartion curves. It can be seen that $FOP_{2\pi(x)}$, which corresponds to the intergration of $FCOOP_{2\pi(x)}$ curve up to the HOMO energy, decreases with increasing CO coverage.

$$= \sum_{k\in\beta}\left(\sum_i 2\,\delta(E-E_i)\sum_{j\in\alpha} C'_{ji}C'_{ki}S'_{jk}\right)$$

$$= \mathrm{FCOOP}_{6\sigma} + \mathrm{FCOOP}_{2\pi(x)} + \mathrm{FCOOP}_{2\pi(y)} + \mathrm{FCOOP}_{5\sigma} + \cdots$$

$$\int_{-\infty}^{E_F} \mathrm{FCOOP}\; dE = \mathrm{FOP} \qquad (8)$$

Results

When the convergence reached for each model clusters, surface Ni atom's energy parameters are moved to lower energy toward the CO 5σ level with increasing CO coverage. This is because the net charge is transferred from Ni surface atoms to adsorbed CO molecules making the surface Ni

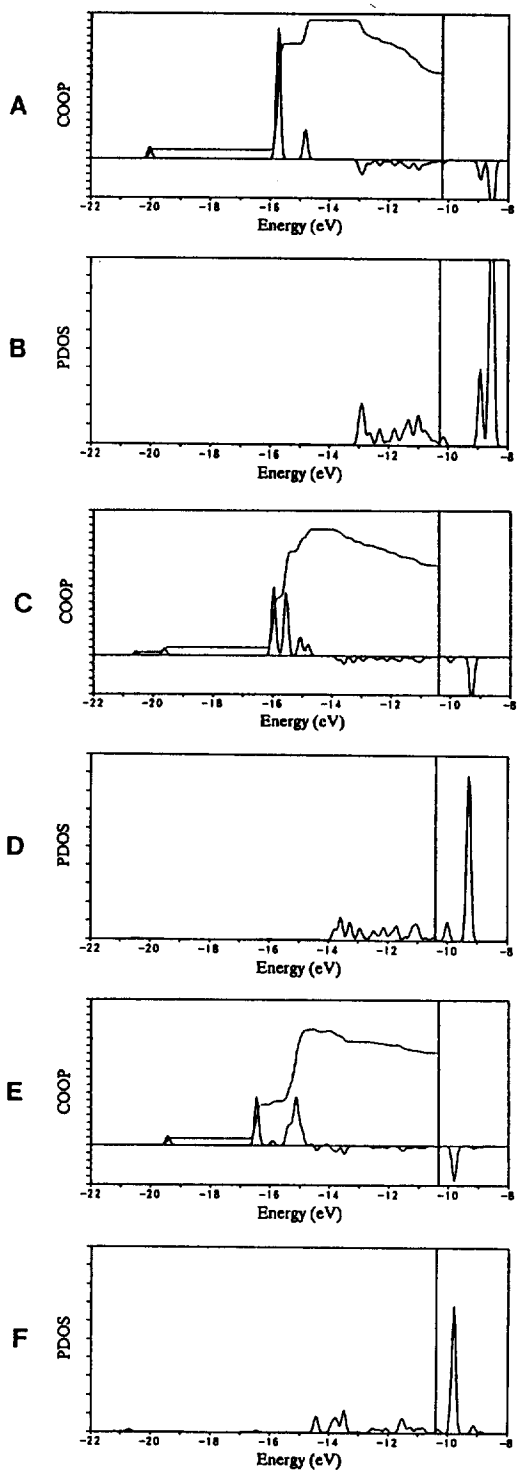

Figure 4. COOP curves between C and O atom, and $PDOS_{2\pi}$ curvers. A. COOP of C-O in model cluster I, B. $PDOS_{2\pi}$ of CO in model cluster I, C. COOP of C-O in model cluster IV, D. $PDOS_{2\pi}$ of CO in model cluster IV, E. COOP of C-O in model cluster V, F. $PDOS_{2\pi}$ of CO in model cluster V. The vertical lines around 10 eV denote the HOMO energies. The dotted line in COOP curve is intergration curve. The height of this intergration curve at the HOMO energy corresponds to the overlap population of C-O bond ($OP_{C\text{-}O}$). The increase of $OP_{C\text{-}O}$ with increasing coverage is not clearly seen in these COOP curves since the differences are small. Table 5 gives numerical values of $OP_{C\text{-}O}$.

Table 7. Results of Calculation for The Pt_{22}-$(CO)_n$ System

No.[a]	$H_{ii}(d)$[b]	$FOP_{2\pi(x)}$[c]	$FOP_{2\pi(y)}$[c]	$FOP_{5\sigma}$[c]	$<n_{2\pi}>$[d]	$OP_{C\text{-}O}$[e]
VI	−12.94430	0.12340	0.12340	0.41231	0.3774	1.2364
VII	−12.84643	0.12571	0.12589	0.41093	0.3903	1.2330
VIII	−12.45478	0.13338	0.13315	0.39302	0.4427	1.2130

[a] CO coverage increases as one goes down the column. see Figure 2. [b] Converged H_{ii} values of the d-orbital of Pt atom at surface center. [c] FOP is defined in Eq. (6) and (7). As coverage increases, $FOP_{2\pi(x)}$ and $FOP_{2\pi(y)}$ increases while $FOP_{5\sigma}$ decreases because the surface Pt valence band moves away from CO 5σ toward CO 2π*. [d] Partial electron occupation numbers of CO 2π* lebel. [e] Overlap population between C and O atom. Decrease of $OP_{C\text{-}O}$ means the red shift of C-O stretching frequency with increasing coverage. $OP_{C\text{-}O}$ of free CO molecule is 1.3269.

atoms to be positive. The extent of CO 2π*-Ni(111) interaction is larger than that of CO 5σ-Ni(111) interaction for CO/Ni(111) system, which results in the net charge flow from Ni surface to adsorbed CO. A single CO molecule, however, takes less charge from Ni cluster although Ni cluster becomes more positive as a whole with increasing CO coverage as can be seen in Table 6. This reduced charge transfer to a single CO molecule results in an increase of C-O overlap population as the CO coverage increased because the partial electron occupation of 2π* is reduced. Increase of C-O overlap population is conceived as the blue shift of C-O stretch frequency. Some authors[56,57] have attempted a correlation between calculated overlap populations and experimental vibrational frequency data. And others[58,59] have proposed the simple relationship between effective electrom occupation of CO 2π* and vibrational frequency. No attempt is made here, however, to use such correlation data to obtain quantitative results because different computational details would give significantly different values.

As the coverage increases, Ni surface valence band shifts to lower energy leading to a weaker perturbative interaction between CO 2π* level and Ni substrate d-band because the gap between the two increases. This shift of metal valence band reduces the magnitude of $FOP_{2\pi(x)}$ and $FOP_{2\pi(y)}$ which represent the contribution of CO $2\pi(x)^*$ and $2\pi(y)^*$ to bond strength between metal substrate and adsorbed CO. $FCOOP_{2\pi(x)}$ or $FCOOP_{2\pi(y)}$ curve shows why $FOP_{2\pi(x)}$ or $FOP_{2\pi(y)}$ is decreased as coverage increased. Only the $FCOOP_{2\pi(x)}$ curve is shown in Figure 3 because the $FCOOP_{2\pi(y)}$ curve has the same shape by symmetry. As the large positive peaks at around −12.8 eV of Figure 3A move to lower energy around −14.5 eV of Figure 3C with increasing coverage, their heights are reduced.

The weaker perturbative interation between metal substrate and CO 2π* with increasing CO coverage result in the reduced net charge transfer from Ni surface to a single CO molecule, and then, the bule shift of C-O stretching frequency. $PDOS_{2\pi}$ and $COOP_{C\text{-}O}$ curves given in Figure 4 shows this effects. As the peaks around −12.8 eV of Figure 4B shift to lower energy around −14.5 eV of Figure 4F, the intergration of $PDOS_{2\pi}$ curve up to the HOMO energy, which is electron occupation number of CO 2π*, is reduced. The $<n_{2\pi}>$ values given in Table 5 shows this reduction of electron occupation number of CO 2π* with increasing coverage explicitly. With increasing coverage, in summary, CO 2π* interacts less strongly with metal d-band, smaller area of CO 2π* band below the Fermi level, smaller elctron occupation numbers of CO 2π* level, and then the blue shift of C-O vibrational frequency is induced. As already mentioned, the blue shift of C-O stretching frequency with increasing coverage for CO/Ni system has been observed in IRAS and HREELS experiments.[18,19]

Table 8. Net Charge[a] of Pt_{22} and CO Fragment in The Pt_{22}-$(CO)_n$ System

No.	Pt_{22}	Center CO	Boundary CO
VI	−0.2147	+0.2147	−
VII	−0.3854	−	+0.1927
VIII	−0.5944	+0.1102	+0.0807

[a] The definition of net charge is given in Eq. (2). Sum of the net charges of Pt_{22}, center CO, and boundary CO multiplied by its number becomes zero because the total systems are neutral model clusters.

As the CO coverage of Pt surface increases, on the other hand, surface Pt atom energy parameters (H_{ii}) move to higher energy toward CO 2π* because the direction of net charge transfer is opposite to the case of CO/Ni(111) system. A single CO molecule on Pt surface becomes less positive with increasing CO coverage, while the Pt substrate becomes more negative as can be seen in Table 8. It is explained as follows. As the Pt surface valence band shifts to higher energy with increasing coverage, the energy gap between Pt d-band and CO 2π* level decreases leading to a stronger perturbative interaction between the two. Simultaneously, the interaction between the Pt d-band and CO 5σ level decrease. In other word, the back-donation from Pt surface to CO molecule increases and the donation from CO to Pt surface decreases simultaneously as the coverage increased. The coverage dependent behavior of $FOP_{2\pi(x)}$, $FOP_{2\pi(y)}$, and $FOP_{5\sigma}$ given in Table 7 supports this view. Overlap population between C and O atom decreases slightly with increasing CO coverage as can be seen in Table 7, which means red shift of C-O stretching frequency.

The binding energies of a CO molecule adsorbed on Ni (111) surface of 1-fold, 2-fold, and 3-fold site are calculated using the metal substrates of model cluster I-V after fixing their energy parameters according to the various CO coverage. On the Ni_{19}(I) and Ni_{19}(II) cluster which simulate a very low CO coverage, the CO molecule adsorbed on the 3-fold site is calculated to be the most tightly bound species. CO adsorbed on 2-fold site is calculated to be the most tightly bound species on the Ni_{19}(III) and Ni_{19}(IV) which simulate

Table 9. Calculated Binding Energies[a] (eV) of CO Molecule Adsorbed on Each Adsorption Site of The Ni_{19} Clusters. Their Energy Parameters (H_{ii}) of Consistuent Ni Atoms are Same as That of Converged Model Clusters

No.	1-fold	2-fold	3-fold
Ni_{19}(I)	3.482	3.634	3.649
Ni_{19}(II)	3.416	3.584	3.624
Ni_{19}(III)	3.418	3.575	3.541
Ni_{19}(IV)	2.962	3.007	2.893
Ni_{19}(V)	2.350	2.290	2.262

[a]Binding energy is calculated as follows. $BE = E(Ni_{19}) + E(CO) - E(Ni_{19}-CO)$.

intermediate CO coverage, and the CO adsorbed on 1-fold site of the Ni_{19}(V) which simulates highest CO coverage is the most tightly bound species.

This behavior of the adsorption site preference of CO molecule adsorbed on Ni(III) surface given in Table 9 is in agreement with experiment. It has been reported that a continuous conversion from the 3-fold to 2-fold, and then, finally to 1-fold site coordinated CO on Ni(111) surface occurs with increase in CO coverage.[18,19]

One suggestive results lies in the work of Garfunkel[60] *et al.*, showing a shift of CO from 1-fold to 2-fold and possibly 3-fold sites on Pt(111) on increasing the coverage of coadsorbed potassium atoms. Ray and Anderson[24] explained this result by using MO theory. They predicted the shift of CO to higher coordination sites to take place as a result of the destabilization of the Pt valence band due to charge transfer from the coadsorbed potassium. As Ray and Anderson show, strong $2\pi^*$ mixing favors high coordination sites and strong 5σ mixing favors the 1-fold site on Pt(111), which explains the shift to high coordination sites when CO and K are coasorbed. While electron transfer from the CO 5σ to the metal decreases, the back-donation from the metal to CO $2\pi^*$ increases with the shift of Pt valence band to higher energy. With this upward shift of Pt valence band, the metal *d*-band moves toward CO $2\pi^*$ and the gap between the $2\pi^*$ level of CO and metal *d*-band decreases leading to a stronger perturbative interaction between the two. In other word, the charge transferred from electropositive adsorbate to metal surface induces the CO molecule to prefer higher coordination site.

The CO molecules adsorbed on Pt surface can be thought as weakly electropositive species and CO adsorbed on Ni surface can be thought as electronegative species. So, different behavior of the coverage dependent adsorption site change of Co/Ni(111) and CO/Pt(111) system may have same origin, the direction of charge transfer, if we accept the Anderson's proposal. It seems really do for the CO/Ni(111) system as can be seen in Table 9. For the CO/Pt(111) system, however, we cannot find consistent behavior of binding energy between 1-fold and 2-fold site with increaing CO coverage except the decrease of difference of binding energy between 1-fold and 2-fold site CO.

The relative amounts of the 5σ donation and the $2\pi^*$ backdonation also manifest themselves in the change of the metal work function φ with CO coverage. Donation of electrons to the metal results in a decrease in φ, while back-donation

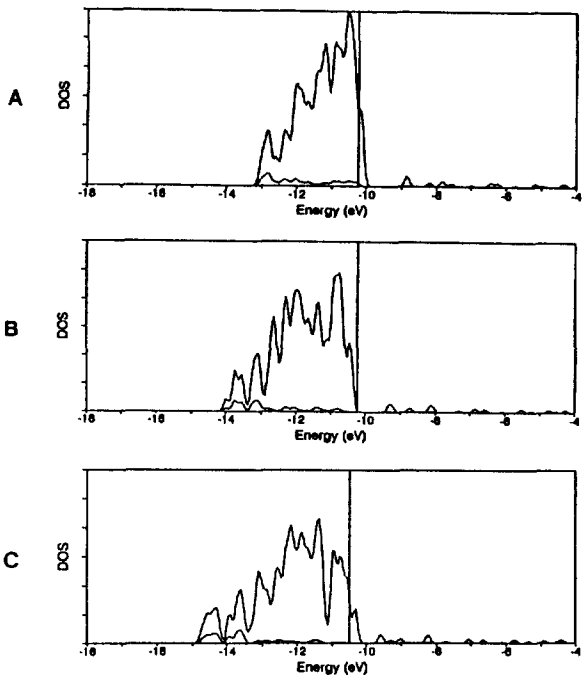

Figure 5. Total DOS (dotted lines) and PDOS of a surface Ni atom (solid lines) for CO/Ni(111) system. A. Ni_{19}(I), B. Ni_{19}(IV), C. Ni_{19}(V). The vertial lines around 10 eV denote the HOMO energies. As the coverage increased, PDOS curves shift to lower energy since the surface Ni atoms are stabilized due to the charge transfer compared with the second layer Ni atoms. In other words, Ni surface atoms become more positive compared with the second layer Ni atoms.

leads to an increase in φ. Therefore, the sign of the work function change $\Delta\varphi$ indicates the direction of the net charge transfer between adsorbate and metal. The work function φ of a metal consists of two parts. The first component originates from the surface dipole *D*, while the second portion is related to the bulk Fermi energy or chemical potential ε_f of an electron[61]:

$$\varphi = D - \varepsilon_f \tag{9}$$

The change in φ after adsorption can be attributed to change in *D*.[61] The ε_f, often termed the internal contribution to the work function, is determined solely by the bulk properties of the solid.[39] The surface dipole layer has a thickness of the order of 2-3 Å. A simulation of the surface dipole layer would require a metal slab of tens of atomic layers.

In our model calculation for the CO/Ni(111) system, *d*-orbital energies of the surface Ni atoms shift to lower energies by about 1.65 eV with increasing CO coverage as can be seen in the first column of the Table 5. The HOMO energy of the Ni_{19} cluster, however, was found to shift to lower energy by only 0.35 eV. This is because the Ni surface atoms which interact directly with adsorbed CO molecules become more positive compared with second layer Ni atoms as CO coverage increases. It is the lower energy part of DOS curve that shift to lower energy with increasing CO coverage as can be seen in Figure 5. This lower part of DOS curve is mainly contributed from surface Ni atoms. This can be conceived as the formation of surface dipole layer having the orientation of increasing metal work function φ. In the case

of CO/Ni(111), it has been reported that $\Delta\varphi$ values increase almost linearly up to certain exposure, beyond which the CO sticking coefficient starts to drop and CO desorption occurs.[63]

In the case of CO/Pt(111), it has been reported that the work function φ decreases after CO adsorption ($\Delta\varphi<0$). According to the work function measurements[64,65], the initial decrease of $\Delta\varphi$ is followed by a minimum at $\theta_{CO}<0.5$. The final value $\Delta\varphi$ at saturation coverage arrives at about 50 meV by changing the sign of $\Delta\varphi$. Etrl *et al.*[64] explained this dramatic change of $\Delta\varphi$ by assuming that, up to a coverage corresponding to the minimum of $\Delta\varphi$, the CO molecules occupy the 1-fold site with a small positive dipole moment (C^-O^+). As the coverage increases, the adsorbed layer is compressed to occupy the 2-fold sites, on which the CO molecules have zero dipole moment.

In our model calculation for the CO/Pt(111) system, the increase of net charge flow from the CO molecules of 1-fold site to Pt surface with increasing CO coverage makes Pt substrate surface to be more negative. This could be related to the initial decrease of metal work function.

Discussion

In this study, coverage dependent C-O stretching frequency shift, adsorption site conversion, and metal work function change are attributed to the charge transfer between metal surface and adsorbate. For CO/Ni(111) system, net charge transfer from Ni surface to chemisorbed CO molecules makes surface Ni atoms be more positive with increasing coverage, and lowers Ni surface valence band. This leads to a weaker interaction between metal surface valence band and CO $2\pi^*$ MO, less charge transfer to a single CO molecule, and the bule shift of C-O stretching frequency. Further increase of coverage induces the conversion of 3-fold site CO to lower coordination site as well as the blue shift of C-O stretching frequency. This whole process is accompanied by the continuous increase of the metal work function.

The transformation of 3-fold site to 2-fold site of CO on Ni(111) surface is completed when θ_{CO} is about 0.16.[18,19] The average CO-CO distance at this coverage is around 6 Å. It is hard to believe that CO-CO direct interaction is turned on at this low CO coverage. This interconversion should, therefore, be initiated by some long-range through-metal interaction. Sung and Hoffmann[66] has reported that CO-CO direct interaction is turned on at CO-CO distance around 3.29 Å. In our model cluster IV, CO-CO distance is 3.32 Å. At this CO-CO distance, binding energy between CO molecules is calculated to be −0.0029 eV (very weak repulsion), and FOP between CO molecules is 0.0108. Overlap populations between C and O atom are 1.3441 for CO at center and 1.3572 for CO at boundary; which correspond to the decrease of 1.5% and 0.5% compared with 1.3641 of free CO molecule. So, CO-CO direct interaction is negligible in our model cluster except model V.

It has been reported that the simultaneous coexistence of 2-fold and 3-fold coordinated CO species on Ni(111) surface at a very low CO coverage is accompanied by a fast site-interconversion process which is coverage and temperature dependent.[19,42] The slight blue shift of the 3-fold CO stretching band with increasing coverage, in spite of the concomitant depopulation of these sites, implies that only chemical interactions are responsible for the observed blue shift. In other words, blue shift caused by dipole-dipole coupling, if exists, would be turned off as CO coverage increased since no dipole coupling is possible between 2-fold CO and 3-fold CO.

The original chemical effect model for coverage dependent CO stretching frequency shift observed on supported metal catalysts has been proposed by Blyholder,[3] who argued that as coverage increased, the increasing competition for metal *d*-electrons would lead to a reduced back-donation per CO molecule, an increased C-O force constant, and a concomitant increase in vibrational frequency. This rationale should, however, be considered with care. Transition metal is highly conductive and its surface is a kind of electron reservoir. If one uses a very small cluster to simulate surface phenomena, finite numbers of electrons in that small cluster would result in the reduction of electron transfer to a single CO molecule as the number of adsorbed CO is increased. In that case, it can not be a good model for the surface, although it may be a model for a transition metal carbonyl complex.

In our calculation, the decrease of electron occupation number of CO $2\pi^*$ level with increasing coverage is caused through the weakening of the interaction between CO $2\pi^*$ and Ni *d*-band due to the stabilization of surface Ni atom energy parameters. It is the project density of states (PDOS) of surface that responds to the CO coverage. Total density of states (DOS) and the Fermi level (HOMO energy) respond weakly to coverage as can be seen in Figure 5. Fermi level of each model clusters lies within the range of 0.35 eV, compared with the 1.65 eV shift of surface Ni *d*-band. The changes of these bulk properties will be smaller if we have used a thicker slab.

The coverage dependent frequency shift of CO on Ni(111) is found to be induced through the metal mediated CO-CO indirect interaction in this work. The CO-CO direct interaction will, however, be turned on above a certain coverage. In that case, red shift due to the broadening of CO $2\pi^*$ level *via* CO-CO direct interaction will begin to compete with blue shift due to the metal mediated CO-CO indirect interaction. So, C-O stretching frequency probably increases with increasing coverage and then decrease when the coverage exceeds a certain value. Surnev *et al.*[19] has reported similar behavior for 1-fold CO on Ni(111) surface through IRAS experiment. This competition between the metal mediated indirect interadsorbate interaction and direct interadsorbate interaction requires further study.

Acknowledgements. This work has been supported by the Korea Science and Engineering Foundation.

References

1. G. Broden, T. N. Rhodin, C. F. Brucker, R. Renbowand, and Z. Hurych, *Surf. Sci.*, **59**, 593 (1976).
2. E. W. Plummer, C. T. Chen, W. K. Ford, W. Eberhardt, R. P. Messmer, and H. J. Frennd, *Surf. Sci.*, **158**, 58 (1985).
3. G. Blyholder, *J. Phys. Chem.*, **68**, 2772 (1964).
4. H. Pfnur, D. Menzel, F. M. Hoffmann, A. Ortega, and A. M. Bradshaw, *Surf. Sci.*, **93**, 431 (1980).

5. A. M. Bradshaw and F. M. Hoffmann, *Surf. Sci.*, **72**, 513 (1978).
6. J. C. Campuzano and R. G. Greenler, *Surf. Sci.*, **83**, 301 (1979).
7. K. Horn and J. Pritchard, *Surf. Sci.*, **55**, 70 (1976).
8. K. Horn, M. Hussain, and J. Pritchard, *Surf. Sci.*, **63**, 244 (1979).
9. B. E. Hayden, K. Kretzschmar, and A. M. Bradshaw, *Surf. Sci.*, **155**, 553 (1985).
10. G. D. Mahan and A. A. Lucas, *J. Chem. Phys.*, **68**, 1344 (1979).
11. B. N. J. Persson and R. Rydberg, *Phys. Rev.*, **B24**, 6954 (1981).
12. B. N. J. Persson and A. Liebsch, *Surf. Sci.*, **110**, 356 (1981).
13. B. E. Hayden, *Vibrational Spectroscopy of Molecules on Surface:* "Reflection Absorption Infrared Spectroscopy", Chap. 7, ed., by J. T. Yates, Jr. and T. E. Madey, Pleum Press, New York (1987).
14. J. C. Campuzano and R. G. Greenler, *Surf. Sci.*, **83**, 301 (1979).
15. J. C. Bertolini and B. Tardy, *Surf. Sci.*, **102**, 131 (1981).
16. M. Trenary, K. J. Uram, and J. T. Yates, Jr., *Surf. Sci.*, **157**, 512 (1985).
17. S. L. Tang, M. B. Lee, Q. Y. Yang, J. D. Beckerle, and S. T. Ceyer, *J. Chem. Phys.*, **84**, 1876 (1986).
18. J. G. Chen, W. Erley, and H. Ibach, *Surf. Sci.*, **223**, L891 (1989).
19. L. Surnev, Z. Xu, and J. T. Yates, Jr., *Surf. Sci.*, **201**, 1 (1988).
20. D. G. Carroll, A. T. Armstrong, and S. P. McGlynn, *J. Chem. Phys.*, **44**, 1865 (1966).
21. A. T. Armstrong, D. G. Carroll, and S. P. McGlynn, *J. Chem. Phys.*, **47**, 1103 (1967).
22. A. B. Anderson and E. Yeager, *Chem. Phys. Lett.*, **82**, 130 (1981).
23. N. K. Ray and A. B. Anderson, *J. Phys. Chem.*, **86**, 4851 (1982).
24. N. K. Ray and A. B. Anderson, *Surf. Sci.*, **125**, 803 (1983).
25. S. P. Mahandru and A. B. Anderson, *J. Am. Chem. Soc.*, **107**, 844 (1985).
26. A. B. Anderson and Md. K. Awad, *J. Am. Chem. Soc.*, **107**, 7854 (1985).
27. B. E. Hayden and A. M. Bradshaw, *Surf. Sci.*, **125**, 787 (1983).
28. E. Schweizer, B. N. J. Persson, M. Tüshaus, D. Hoge, and A. M. Bradshaw, *Surf. Sci.*, **213**, 49 (1989).
29. I. J. Malik and M. Trenary, *Surf. Sci.*, **214**, L240 (1989).
30. B. N. J. Persson and R. Rydberg, *Phys. Rev. B*, **40**, 10273 (1989).
31. B. N. J. Persson M. Tüshaus, and A. M. Bradshaw, *J. Chem. Phys.*, **92**, 5034 (1990).
32. S. D. Kevan, R. F. Davis, D. H. Rosenblatt, J. G. Tobin, M. G. Mason, and D. A. Shirley, *Phys. Rev. Lett.*, **46**, 1629 (1981).
33. M. Passler, A. Ignatiev, F. Jona, D. W. Jepsen, and P. M. Marcus, *Phys. Rev. Lett.*, **43**, 360 (1979).
34. S. T. Tong, A. Maldonada, C. H. Li, and M. A. van Hove, *Surf. Sci.*, **94**, 73 (1980).
35. S. Anderson and J. B. Pendry, *J. Phys. C.*, **13**, 3547 (1980).
36. P. Li and M. D. Curtis, *J. Am. Chem. Soc.*, **111**, 8279 (1989).
37. J. J. Maj, A. D. Rae, and L. F. Dahl, *J. Am. Chem. Soc.*, **104**, 3054 (1982).
38. M. M. Olmstead and P. P. Power, *J. Am. Chem. Soc.*, **106**, 1495 (1984).
39. Y. T. Wong and R. Hoffmann, *J. Phys. Chem.*, **95**, 859 (1990).
40. A. B. Anderson and S. F. Jen, *J. Phys. Chem.*, **94**, 1607 (1990).
41. J. C. Compuzano and R. G. Greenler, *Surf. Sci.*, **83**, 301 (1979).
42. L. Surnev and Z. Xu, *Surf. Sci.*, **201**, 14 (1988).
43. D. F. Ogletree, M. A. van Hove, and G. A. Somorjai, *Surf. Sci.*, **173**, 351 (1986).
44. R. Jostes, *Theoret. Chim. Acta (Berl.)*, **74**, 229 (1988).
45. J. Howell, A. Rossi, D. Wallace, K. Haraki, and R. Hoffmann, **FORTICON**, QCPE No. 344, Indiana University, Bloomington, Indiana.
46. G. Burns, *J. Chem. Phys.*, **41**, 1521 (1964).
47. J. W. Richardson, W. C. Niuwpoort, R. R. Powell, and W. F. Edgell, *J. Chem. Phys.*, **36**, 1057 (1962).
48. H. Basch and H. B. Gray, *Theoret. Chim. Acta (Berl.)*, **4**, 367 (1966).
49. S. P. McGlynn, L. G. Vanquickenborne, M. Kinoshita, and D. G. Carroll, *Introduction to Applied Quantum Chemistry*, Holt, Rinehart, and Winston, Inc., New York, pp. 423-431 (1972).
50. C. J. Ballhausen and H. B. Gray, *Molecular Orbital Theory*, W. A. Benjamin, Inc., New York, p. 120 (1964).
51. D. A. Brown and A. Owens, *Inorg. Chimica Acta.*, **5**, 675 (1971).
52. R. Munita and J. R. Letelier, *Theoret. Chim. Acta (Berl.)*, **58**, 167 (1981).
53. C. M. Rohlfing and P. J. Hay, *J. Chem. Phys.*, **83**, 4641 (1985).
54. A. E. Stevens, C. S. Feigele, and W. C. Lineberger, *J. Am Chem. Soc.*, **104**, 5026 (1982).
55. R. Hoffmann, *Rev. Mod. Phys.*, **60**, 601 (1988).
56. P. Politzer and S. D. Kasten, *J. Phys. Chem.*, **80**, 385 (1976).
57. T. S. Kusuma and A. L. Companion, *Surf. Sci.*, **195**, 59 (1988).
58. E. J. Baerands and P. Ros, *Mol. Phys.*, **30**, 2940 (1975).
59. S. Holloway and J. K. Norskov, *J. Electroanal. Chem.*, **161**, 193 (1984).
60. E. L. Garfulkel, J. E. Crowell, and G. A. Somorjai, *J. Phys. Chem.*, **86**, 310 (1982).
61. V. Heine and C. H. Hodges, *J. Phys. C: Solid State Phys.*, **5**, 225 (1972).
62. D. P. Woodruff and T. A. Delchar, *Modern Techniques of Surface Science;* Cambridge University Press: Cambridge, p. 25, 356, 361 (1986).
63. K. Christmann, O. Schober, and G. Ertl, *J. Chem. Phy.*, **60**, 4719 (1974).
64. G. Ertl, M. Neumann, and K. M. Streit, *Surf. Sci.*, **64**, 393 (1977).
65. P. R. Norton, J. W. Goodale, and E. B. Selkirk, *Surf. Sci.*, **83**, 189 (1979).
66. S. S. Sung and R. Hoffmann, *J. Am. Chem. Soc.*, **107**, 578 (1985).